Bifurcation and chaos in the double-well Duffing–van der Pol oscillator: Numerical and analytical studies

A. Venkatesan and M. Lakshmanan
Department of Physics, Centre for Nonlinear Dynamics, Bharathidasan University, Tiruchirappalli 620 024, India
(Received 3 June 1997)

The behavior of a driven double-well Duffing–van der Pol oscillator for a specific parametric choice ($|\alpha|=\beta$) is studied. The existence of different attractors in the system parameters f-ω domain is examined and a detailed account of various steady states for fixed damping is presented. The transition from quasiperiodic to periodic motion through chaotic oscillations is reported. The intervening chaotic regime is further shown to possess islands of phase-locked states and periodic windows (including period-doubling regions), boundary crisis, three classes of intermittencies, and transient chaos. We also observe the existence of local-global bifurcation of intermittent catastrophe type and global bifurcation of blue-sky catastrophe type during the transition from quasiperiodic to periodic solutions. Using a perturbative periodic solution, an investigation of the various forms of instabilities allows one to predict Neimark instability in the f-ω plane and eventually results in the approximate predictive criteria for the chaotic region. [S1063-651X(97)05611-0]

PACS number(s): 05.45.+b

I. INTRODUCTION

The Duffing–van der Pol (DVP) oscillator

$$\ddot{x}-\mu(1-x^2)\dot{x}+\alpha x+\beta x^3=f\cos\omega t,\quad \mu>0, \tag{1}$$

where the overdot represents a derivative with respect to time, is a ubiquitous nonlinear differential equation that makes its presence in physical, engineering, and even biological problems [1–7]. It is a generalization of the classic van der Pol oscillator equation. It can be considered in at least three physically interesting situations, wherein the potential $V(x)=\alpha x^2/2+\beta x^4/2$ is a (i) single well ($\alpha>0,\beta>0$), (ii) double well ($\alpha<0,\beta>0$), or (iii) double hump ($\alpha>0,\beta<0$). Each one of the above three cases has become a classic central model to describe inherently nonlinear phenomena, exhibiting a rich and baffling variety of regular and chaotic motions.

Chaotic motion in system (1) with a single-well–type restoring force was investigated by Ueda and Akamatsu [8] as a model of negative resistance oscillator and later on was studied by a number of other authors [9–12], who noted symmetry breaking of attractors and the onset of chaotic dynamics. Bountis *et al.* [11] have investigated the nonintegrability of a family of DVP oscillators by studying analyticity properties of the solution in the complex time plane and proved that an infinitely sheeted structure exists in this system. Rajasekar, Parthasarthy, and Lakshmanan [13] pointed out that the DVP oscillator with a double-well potential exhibits Smale horseshoe chaos when transverse intersections of the homoclinic orbits occur. Further, Kao and Wang [14] had analog simulated the DVP oscillator with a double-hump potential and discussed the various mode-locking, multiple hysteresis, period-doubling route to chaos, intermittent hopping, and crises phenomena.

Recently, Szemplinska-Stupnika and Rudowski [12] reported that a single-well–type DVP oscillator exhibits chaotic motion between two types of regular motion, namely, periodic and quasiperiodic oscillations, in the prinicipal resonance region for a specific value of the parameter f ($=1.0$) and a range of ω values (0.8–1.0). Also they have obtained a perturbative solution for the periodic oscillation and carried out a stability analysis of such a solution to predict Neimark bifurcation. However, no such analysis exists for the important case of the double-well–type DVP oscillator so far in the literature, which is atypical in the sense that even in the absence of forcing it shows the existence of multiple attractors [6,7].

Considering the DVP oscillator with a double-well–type restoring force in the form

$$\ddot{x}-\mu(1-x^2)\dot{x}-|\alpha|x+\beta x^3=f\cos\omega t,\ \beta>0, \tag{2}$$

we notice that the three equilibrium points of the system (2) for $f=0$ correspond to $-|\alpha|x+\beta x^3=0$, so that we have the stable fixed points $x_{1,2}^{(s)}=\pm\sqrt{|\alpha|/\beta}$ and the unstable fixed point that is hyperbolic at $x_0^{(u)}=0$. Actually, $x_{1,2}$ are elliptic points for $|\alpha|=\beta$ and become stable foci for $|\alpha|>\beta$, while they are unstable foci for $|\alpha|<\beta$. As a result, the system (2) exhibits a large-orbit motion, which always encircles all the three equilibrium points for the case $|\alpha|=\beta$. As far as $|\alpha|>\beta$ is concerned, the system exhibits both small-orbit, that is, oscillation around any one of the stable fixed points, and large-orbit motion, depending upon the values of the other control parameters and also initial conditions.

In this paper we undertake an investigation of the dynamics of the double-well DVP oscillator (2) and show that it is a rich dynamical system, possessing a vast number of regular and chaotic steady states. In particular, considering the special case $|\alpha|=\beta$ (the case $|\alpha|\neq\beta$ is even richer and the results will be presented separately [16]), we bring out the existence of a transition from quasiperiodic to periodic motion in the f-ω parameter space *via chaotic motion*. The different features we observe are that in the chaotic sea there are many isles of periodic and phase-locked states, which exhibit period-doubling phenomena, intermittencies, crises, etc., along with regions of transient chaos, corresponding to local bifurcations. In addition, there are also transitions from

quasiperiodicity to period-T orbits corresponding to global bifurcation of blue-sky and local-global bifurcation of intermittent catastrophes. We also present a perturbative approach to the study of bifurcations that occur near the principal resonance. The analysis allows us to derive the algebraic equations for the instability boundaries.

The plan of the paper is as follows. In Sec. II we present the numerical results for different steady states, bifurcation routes, and chaos for system (2). In Sec. III we develop a perturbative solution and obtain expressions for the stability regions and compare them with numerical results. Then we compare the results with the dynamics of the double-well Duffing oscillator in Sec. IV. Finally, Sec. V summarizes our results.

II. NUMERICAL RESULTS

Equation (2) is numerically integrated using the fourth-order Runge-Kutta algorithm with adaptive step size with parameter values fixed at $|\alpha|=0.5$, $\beta=0.5$, and $\mu=0.1$ in order to study the large-orbit behavior mentioned in the Introduction. The transitions are also characterized by tracing the time evolutions, phase portrait, Poincaré map, Fourier spectrum, and Lyapunov exponents. For identifying different steady states, the dynamical transitions are traced out by two different scanning procedures: (i) varying ω at a fixed f (frequency scanning) and (ii) varying f at a fixed ω (amplitude scanning). The resulting phase diagram in the f-ω parameter is shown in Fig. 1. The diagram covers the transition thresholds in the region of principal and superharmonic resonances $0.4<\omega<1.0$ and the forcing strength lying in the region $0.0<f<0.2$. The various features in the phase diagram are summarized and the dynamical transitions of the attractors are elucidated in the following.

A. Phenomena of steady states

One observes that Eq. (2) admits the free-running solution when the external force is absent ($f=0.0$). When it is present and for low-f values and low-ω values, the frequency of the system becomes incommensurate with the external frequency. Consequently, the system exhibits multifrequency quasiperiodic oscillations. When the value of the external frequency ω exceeds a certain critical value for fixed f, a transition from quasiperiodic to periodic oscillations occurs on increasing ω (see Fig. 1) essentially due to supercritical Neimark bifurcation (see Secs. II B and III). This phenomenon continues until a critical f value ($f\sim0.115$).

On increasing the forcing parameter f further, $f>0.115$, the system exhibits chaotic motion between the two regular motions, that is quasiperiodic and periodic oscillations, within a range of the driving frequency ω. For example, at $f=0.13$, chaotic motion occurs in the region $\omega\in(0.546,0.553)$ [see Fig. 2(a)].

As the forcing parameter f increases further, within a very narrow frequency region, a chaos—periodic windows—chaos type of transition is found to occur between the two regular oscillations. For example, at $f=0.14$, a period-5T solution occurs in the frequency range $\omega\in(0.545,0.551)$ within the chaotic range $\omega\in(0.525,0.553)$ [see Fig. 2(b)]. At $f=0.17$, a period-doubling phenomenon occurs in the window region of the frequency $\omega\in(0.503,0.529)$. In the above range, we note that the period-2 orbit is born at $\omega=0.529$; it undergoes a period-(2×2^m)-doubling bifurcation, finally leading to the onset of chaos as ω decreases [see Fig. 2(c)].

Higher values of the forcing strength f introduce the appearance of a new transition. When this increase is coupled with increasing frequency, the quasiperiodic motion suddenly changes into a phase-locked attractor. As an example at $f=0.19$, the transition from a quasiperiodic oscillation to phase locked states of period-3 orbit occurs at $\omega=0.453$ and this locked state persists in the frequency range $\omega\in(0.453,0.47)$, which is then followed by chaos, reverse period doubling, chaos, and periodic solution [see Fig. 2(d)].

The details of our numerical study are summarized in the f-ω phase diagrams, Fig. 1 and the bifurcation diagrams of Fig. 2. They depict the system parameter region where quasiperiodic, large periodic, and chaotic attractors exist. The curves denoted QP(1), QP(2), and P(1) are the boundaries of the transition from the quasiperiodic to the chaotic state, the quasiperiodic to the periodic state, and the chaotic to the periodic state, respectively. Also, one observes in the entire transition regions very often the coexistence of multiple attractors. Further, beyond the curve P(1), there are some regions that exhibit phase-locked periodic and transient chaotic states. However, in this paper, those states are not discussed in detail.

Various steady states, denoted as 1,2,3, . . . ,15 in Fig. 1, are then illustrated in Fig. 3. Regular attractors are illustrated by their phase portraits and quasiperiodic and chaotic attractors by their Poincaré maps.

The first three points (1)–(3) in Fig. 3 are examples of almost periodic (quasiperiodic) orbits for low values of f. Then points (4)–(15) are essentially located at the principal and superharmonic resonance regions for large values of the forcing parameter $f>0.12$, at increasing driving frequency ω. We observe here the following: a quasiperiodic orbit [point (4)], a period-3T orbit [point (5)], chaotic orbits [points (6) and (7)], period-doubled orbits [points (8) and (9)], chaotic orbits [points (10) and (11)], a period-5T orbit [point (12)], and period-T orbits [points (13)–(15)].

B. Classification of bifurcations

The complicated dynamical behaviors of the DVP oscillator (2) with $|\alpha|=\beta$ due to the presence of the double-well restoring force has been confirmed by the phase diagram as discussed above. From the bifurcation theory point of view, these correspond to several types of bifurcations: secondary Hopf, intermittent, and blue-sky catastrophes, in addition to standard period-doubling bifurcations, which are discussed in the following section.

1. Local bifurcations in the QP(1) region: Secondary Hopf (Neimark) bifurcation

In analogy with the Hopf bifurcation, a bifurcation is expected at a critical value as the limit cycle loses its stability, so that an attracting torus is born. This is the secondary Hopf bifurcation or a Neimark bifurcation [17]. Further, the bifurcated solution can be either stable and supercritical or unstable and subcritical. For the present DVP oscillator (2) with $|\alpha|=\beta$, there is a very large transition region QP(1) corresponding to this secondary Hopf bifurcation. As an ex-

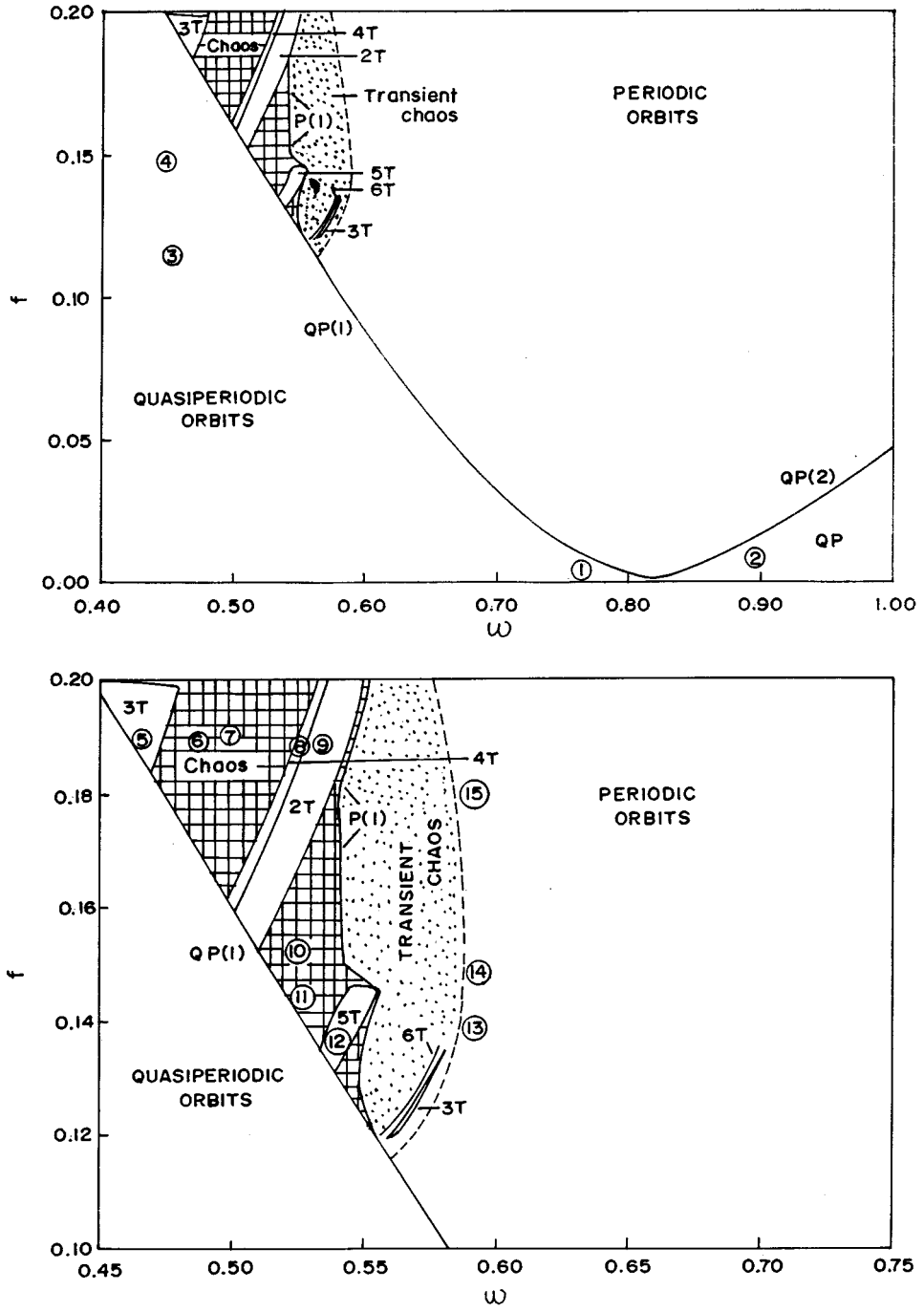

FIG. 1. Regions of different steady states exhibited by the double-well DVP oscillator (2) at $\mu=0.1$.

ample, let us examine the transient process near $f=0.1$. Figure 4 shows the Poincaré maps with values of ω decreasing and with the starting values of x and $\dot{x}$ indicated in parentheses. In Fig. 4(a), for $\omega=0.59$, we see a nodelike convergence to a point, while in Fig. 4(b), for $\omega=0.58$, the convergence has a spiraling character and the rate of convergence is noticeably slower. In Fig. 4(c), at $\omega=0.57$, we see that the system is moving outward from near an unstable fixed point towards the attracting invariant closed curve and the approach is termed supercritical. This is the typical behavior for the curve QP(1) in Fig. 1 for $f<0.10$.

The other nature of Neimark bifurcation, namely subcritical behavior, has also been observed in system (2). For example, at $f=0.15$, the chaotic region exists in the range $\omega \in (0.512,0.551)$ (see Fig. 5). It follows that this narrow strip of chaotic motion is related to the transition from a quasiperiodic to a periodic oscillation via chaotic motion. This transition does not occur in a smooth, continuous way, as is the case when the Neimark bifurcation is a supercritical one, but occurs through a chaotic region. This type of transition has a close resemblance to the Duffing oscillator [15,17,18] case, where it was shown that a lower-frequency band of the chaotic region is related to the saddle-node bifurcation, which causes a sudden change from (to) the T-periodic orbit to (from) the chaotic attractor and transient motions separate the two different steady states. Thus, by analogy, the occur-

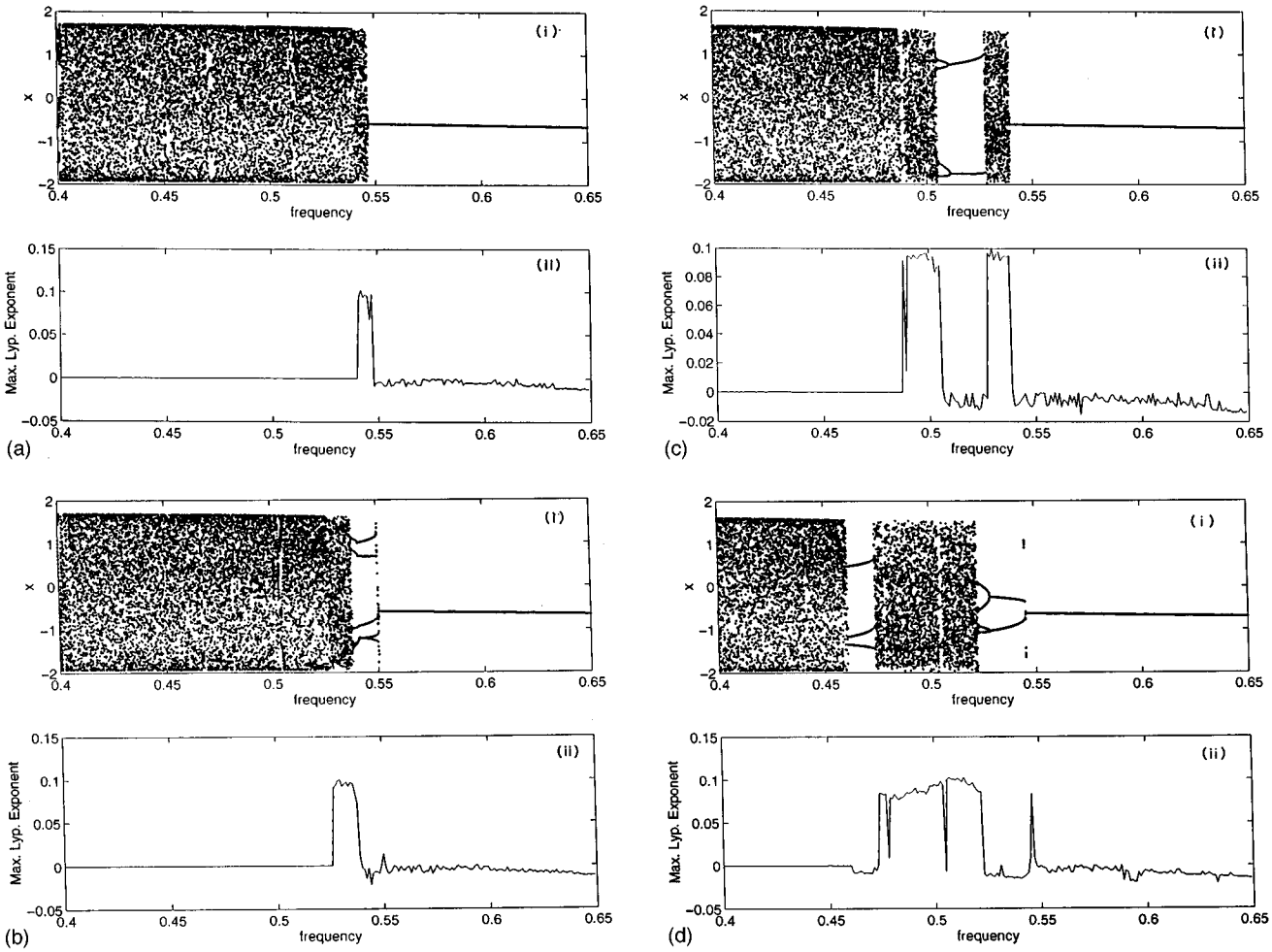

FIG. 2. (i) Bifurcation diagram for maximum amplitude x vs external forcing frequency ω and (ii) Maximal Lypanov exponet λ_{max} vs external forcing frequency ω of system (2). (a) QP—chaos—periodic orbit transitions for $\omega \in (0.4,0.65)$ at $f=0.13$. (b) QP—chaos—periodic windows—chaos transitions for $\omega \in (0.4,0.65)$ at $f=0.14$. (c) QP—chaos—period-doubling window—chaos transitions for $\omega \in (0.4,0.65)$ at $f=0.17$. (d) QP—phase-locked states—chaos—period-doubling windows—chaos transitions for $\omega \in (0.4,0.65)$ at $f=0.19$.

rence of chaotic motion in the region of driving frequency that separates quasiperiodic and periodic oscillations can be interpreted as a subcritical Neimark bifurcation. This type of bifurcation has been reported earlier in Ref. [12] for the single-well DVP oscillator, but the unstable motion corresponds to randomly transitional motion, whereas in the present double-well case this corresponds to a fully chaotic attractor and periodic windows.

2. Local-global bifurcation in the QP(2) region: Intermittent catastrophe

Figure 6 shows the typical Poincaré maps with forcing values $f=0.001\,72$ and $0.001\,73$ at $\omega=0.83$ in the QP(2) region, where a transition from quasiperiodic to periodic motion occurs. In order to lock the quasiperiodic motion to the period-T motion, the Poincaré map points form a closed loop with points progressing more rapidly near the top of the attractor and more slowly where points are visibly dense. As the external force strength is increased, a saddle-node pair develops such that quasiperiodic motion rapidly shrinks to the node, which is near the original attractor. This type of process is prototypical of an intermittent catastrophe [17,19].

3. Global bifurcations in the QP(2) region: Blue-sky catastrophe

As the frequency value is increased to $\omega=0.998$, a different transition process is captured for $f=0.05$. The typical Poincaré map is shown in Fig. 7 with the values of ω at 0.998 and 1 and $f=0.05$. From Fig. 7, we find that a periodic attractor bifurcates to a quasiperiodic attractor that is located inside the other, and the two attractors are typically disjoint and separated in phase space by a finite distance. Furthermore, it is not generic for a quasiperiodic attractor to appear suddenly at the same control threshold where periodic motion vanishes. The quasiperiodic attractor will have existed previously or it will not exist at all; in either case the bifurcation will consist of the periodic attractor simply losing stability: It vanishes into the blue. Such a phenomenon is termed blue-sky catastrophe [17,20] in the literature and this event involves collisions with saddle-type objects.

4. Transitions to chaotic attractors in the V*-shaped region*

We now enumerate the various possible attractors present in the system in the V-shaped region in Fig. 1.

(i) Transient chaos and boundary crises. Chaotic behavior is observed between the boundary of curves QP(1) and P(1)

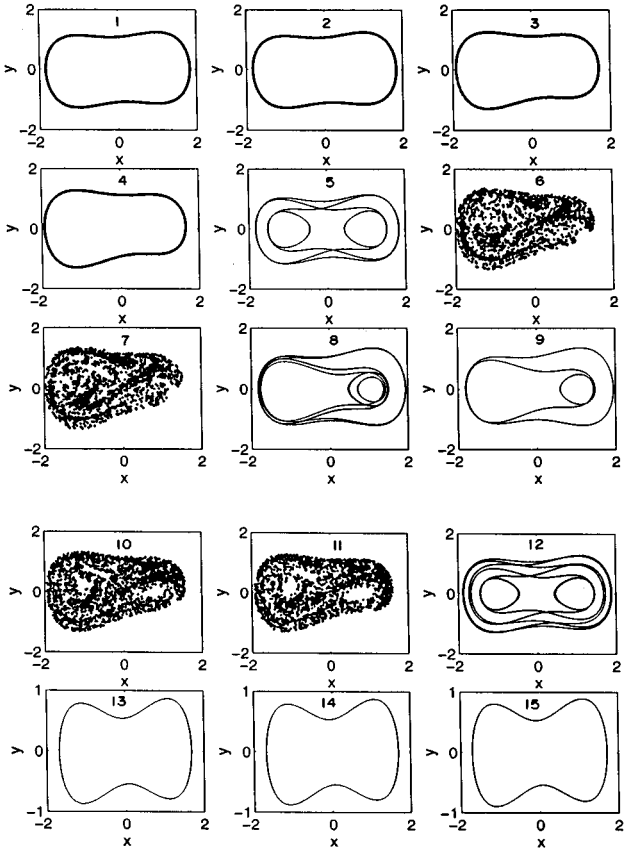

FIG. 3. Various types of steady states at $\mu=0.1$: (1) $f=0.001$, $\omega=0.78$; (2) $f=0.001$, $\omega=0.9$; (3) $f=0.12$, $\omega=0.45$; (4) $f=0.15$, $\omega=0.45$; (5) $f=0.19$, $\omega=0.47$; (6) $\omega=0.515$; (7) $\omega=0.52$; (8) $\omega=0.525$; (9) $\omega=0.53$; (10) $f=0.15$, $\omega=0.54$; (11) $f=0.14$, $\omega=0.53$; (12) $f=0.135$, $\omega=0.54$; (13) $f=0.14$, $\omega=0.58$; (14) $f=0.15$, $\omega=0.58$; (15) $f=0.18$, $\omega=0.58$.

in Fig. 1. Near the boundaries of the curves P(1) and QP(1), the system behaves in a random way, with the trajectory moving in phase space as if it were on a strange attractor. However, after a transient time, the motion settles into a regular attractor, that is, near P(1) it settles into a periodic motion (for example, see Fig. 8), while near QP(1) it settles into a quasiperiodic oscillation. Such a phenomenon is termed transient chaos, which is a precursor to steady-state chaos. Between these two transitional regions, periodic windows, phase-locked states, chaotic attractors, and period-doubling phenomena occur. In addition, the boundary crisis [21] of the chaotic attractor appears as the value of the external frequency increases so that the dynamics corresponds to the curve P(1), where the boundary of the chaotic attractor touches the unstable periodic orbit.

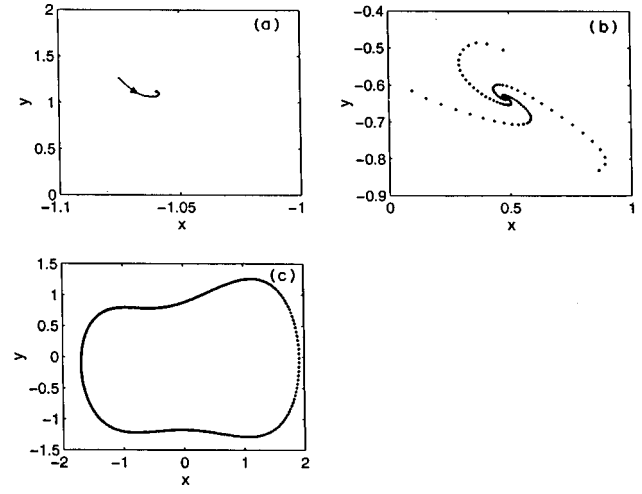

FIG. 4. Trajectories near the Neimark bifurcation for system (2) at $f=0.1$: (a) $\omega=0.59$ (1,1); (b) $\omega=0.59$ (1,1); and (c) $\omega=0.57$ (1,1).

In addition, one observes the interesting fact that in the V-shaped region there exists different parametric values for which intermittency of all three classic types occurs. This seems to be rare in such low-dimensional systems.

(ii) Type-I intermittency. The parameter regions separating the periodic windows inside the V-shaped region correspond to various complicated dynamics including chaos. The precise stability boundary of each window has been found to correspond to a saddle-node instability. As an example, for $f=0.17$, if ω is increased across the saddle-node boundary, type-I intermittency occurs [22–25]. One such intermittency signature is shown in Fig. 9. The average laminar length ($\langle l\rangle$) of this type of intermittency is found to comply with the law $\langle l\rangle\sim\mu^{-\delta}$, with $\delta\sim 0.52\pm 0.001$, where $\mu=\omega-\omega^c$ and ω^c is the bifurcation threshold.

(iii) Type-II intermittency. We showed that two possibilities exist in the QP(1) region when the periodic motion encounters a Hopf bifurcation. Either quasiperiodic motion results if the bifurcation is supercritical or a complicated evolution appears if the bifurcation is subcritical. In the latter case the transition to chaos is found to have an intermittency signature in certain parametric regions. Such an intermittency signature is shown in Fig. 10. A close look into the signature reveals that there are distinct phases of the regular motion that are punctuated by other phases that are apparently chaotic. According to the classical Pomeau-Manneville categorization of different types of intermittencies based on local bifurcations, the present intermittency is of type II since the preceding bifurcation is a Hopf bifurcation [22–25]. The average length $\langle l\rangle$ of the laminar phase of this intermittency is found to comply with the law $\langle l\rangle\sim(1/\mu)^{\delta}$, with $\delta=0.9321$, where $\mu=\omega-\omega^c$ and ω^c is the bifurcation threshold.

(iv) Type-III intermittency. Next we discuss yet another type of route in which the periodic orbits in the periodic windows are seen to undergo an intermittent transition to chaos. One such intermittent motion is shown in Fig. 11, which is a Poincaré time series plot for $f=0.14$ and $\omega=0.538\,02$. It is seen that the motion just before the onset of intermittency is of period-20 orbit, which itself occurred due to the period doubling of the period-10 orbit. The laminar phase of Fig. 11 corresponds to the period-40 orbit along with chaotic bursts. Therefore, this is identified to have arisen out of a subcritical half subharmonic instability, that is, subcritical period doubling. Thus, according to the Pomeau-Manneville classification, this is type-III intermittency [22]. The average length $\langle l\rangle$ of the laminar phase of this intermittency complies with the following scaling law predicted by Pomeau and Manneville: $\langle l\rangle\sim(1/\mu)^{\delta}$, with $\delta=0.9912$, where $\mu=\omega-\omega^c$ and ω^c is the bifurcation threshold.

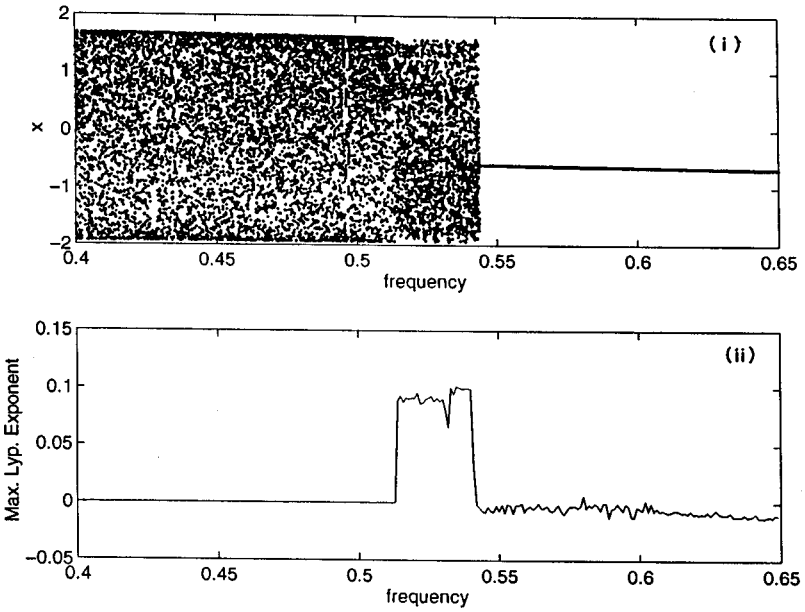

FIG. 5. (i) Bifurcation diagram for maximum amplitude x vs external forcing frequency ω and (ii) Maximal Lypanov exponet λ_{max} vs external forcing frequency ω of system (2). QP—chaos—periodic orbit transitions for $\omega \in (0.4,0.65)$ at $f=0.15$.

III. PERTURBATIVE ANALYSIS

From the numerical studies reported in the previous sections, we observed that the periodic-T orbit within a range of driving frequency ω for low values of f is close to a harmonic function of time. Then, by obtaining a first-order approximate period-T $(=2\pi/\omega)$ solution and analyzing the stability, one can estimate the system parameter domain in which Neimark instability arises, as was done in the case of a single-well DVP oscillator for fixed f and ω in Ref. [12]. Keeping this aim in mind, we look for a periodic solution of Eq. (2) using a perturbative method (with both $|\alpha|$ and β fixed at 0.5). Applying the method of multiple scales [1,26] to Eq. (2), one can obtain the approximate solution about the stable fixed point $x_s=\sqrt{\alpha/\beta}$ in the form

$$x=-\frac{3}{4}a^2+a\cos(\omega t+\phi)+\frac{a^2}{4}\cos 2(\omega t+\phi)$$
$$-\frac{a^2}{3}\mu\sin 2(\omega t+\phi), \tag{3}$$

where

$$a=\frac{f}{\sqrt{[\Omega^2(a)-\omega^2]^2+\left(\frac{3}{2}\mu\omega a^2\right)^2}}, \tag{4}$$

$$\tan\phi=-\frac{\frac{3}{2}\mu\omega a^2}{\Omega^2(a)-\omega^2}, \tag{5}$$

and $\Omega^2(a)=1-\frac{9}{8}a^2$ is the natural frequency of the autonomous conservative system (2) at $\mu=0$ and $f=0$.

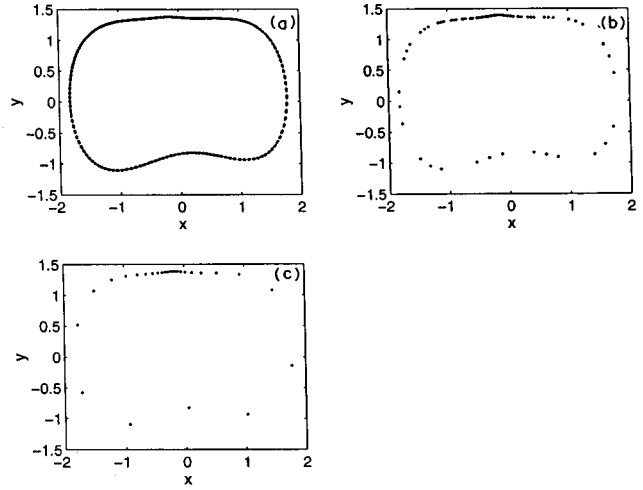

FIG. 6. Poincaré map of the system (2) before and after mode locking for (a) $f=0.001\,72$, (b) $f=0.001\,73$, and (c) $f=0.001\,74$ at $\omega=0.83$.

A. Linear stability analysis

1. Soft-mode instability

In order to examine the stability of the solution (3), we may look at a specific form of instability that manifests itself by an exponential growth with time of the harmonic components in the solution (3). This can be done by adding small disturbances to the amplitude and phase of the solution (3) as

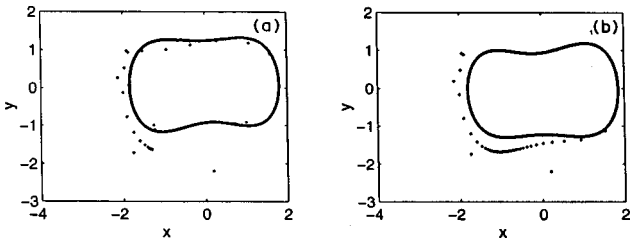

FIG. 7. Poincaré map of the blue-sky disappearance of the periodic attractor in system (2): (a) $\omega=0.998$ and (b) $\omega=1$, at $f=0.05$.

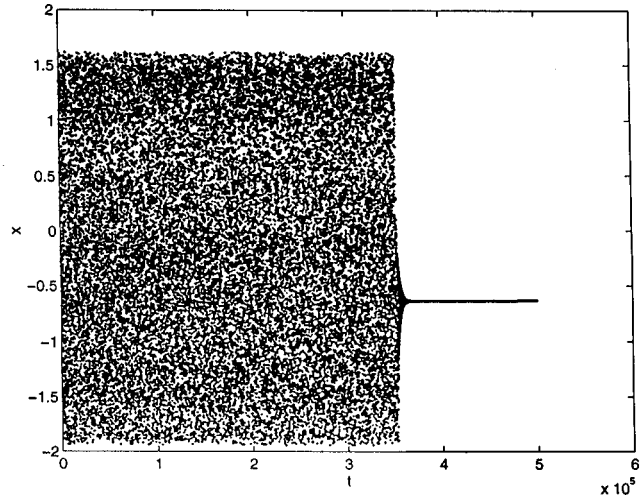

FIG. 8. Trajectories to show transient chaos for $f=0.125$ and $\omega=0.535$.

$$x=-\frac{3}{4}(a+\delta a)^2+(a+\delta a)\cos(\omega t+\phi+\delta\phi)+\frac{(a+\delta a)^2}{4}\cos 2(\omega t+\phi+\delta\phi)-\frac{(a+\delta a)^2}{3}\mu\,\sin 2(\omega t+\phi+\delta\phi). \tag{6}$$

Working out the linearized equation for δa and $\delta\phi$, one ultimately arrives at the following expression, which corresponds to the first-order instability limit:

$$\omega^4+\left(\frac{27}{4}\mu^2a^4-2a^2-2\right)\omega^2+\left(2a^2+\frac{53}{16}a^4+1\right)=0. \tag{7}$$

The above analysis is valid only for a fluctuation having the same frequency as the approximate solution $x(t)$ considered.

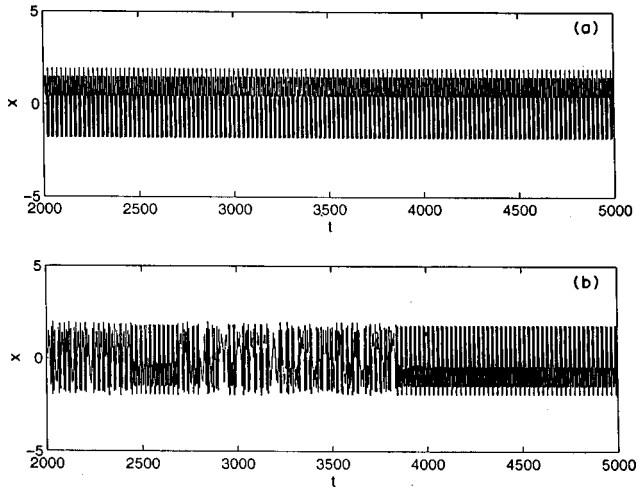

FIG. 9. Signature of type-I intermittency: Time series plot for $f=0.17$ and (a) $\omega=0.526\,01$ and (b) $\omega=0.526\,010\,001$.

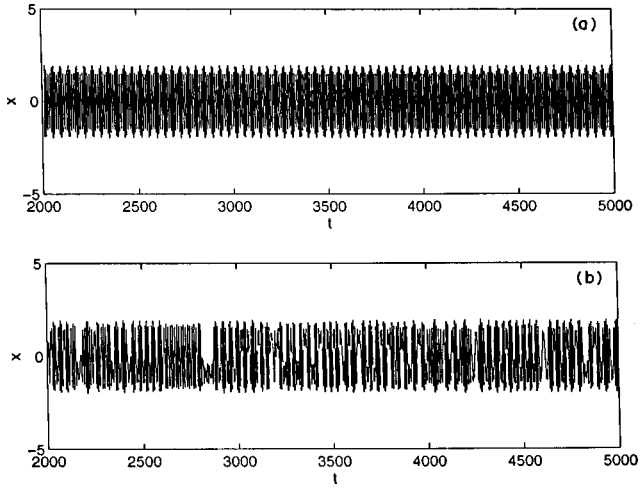

FIG. 10. Signature of type-II intermittency: Time series plot for $f=0.12$ and (a) $\omega=0.5532$ and (b) $\omega=0.5537$.

2. Hard-mode instability

Now we examine another type of instability in which the perturbation may have different harmonic components other than those in $x(t)$. Following the spirit of the work of Szemplinska-Stupnicka and Rudowski [12] let us study, the effect of a small disturbance to $x(t)=\overline{x}(t)$, where $\overline{x}(t)$ is the solution (3), in the form

$$x(t)=\overline{x}(t)+\delta x(t). \tag{8}$$

The linear variational equation for $\delta x(t)$ is then

$$\delta\ddot{x}+P_1(t)\,\delta\dot{x}+P_2(t)\,\delta x=0, \tag{9}$$

where

$$P_1(t)=-\mu\left[1-\left(a_0^2+\frac{a^2}{2}+\frac{a_2^2}{2}+\frac{a_3^2}{2}\right)+2a_0a\,\cos\theta+\left(\frac{a^2}{2}\right)\cos 2\theta+\cdots\right], \tag{10}$$

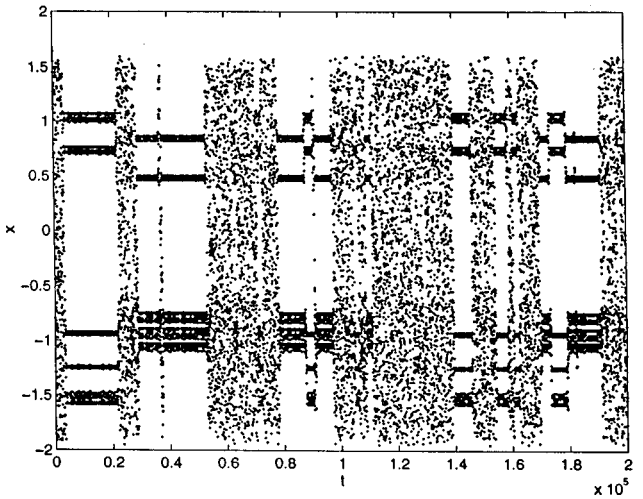

FIG. 11. Signature of type-III intermittency: Poincaré time series plot for $f=0.14$ and $\omega=0.538\,02$.

$$P_2(t)=-|\alpha|+3\beta\left(a_0^2+\frac{a^2}{2}+2a_0a\cos\theta+\frac{a^2}{2}\cos2\theta\right)+2\mu\left[\left(-a_0^2a-\frac{a^3}{4}\right)\omega\sin\theta+a_0a^2\omega\sin2\theta-\frac{a^3}{2}\omega\sin3\theta\right]+\cdots, \tag{11}$$

with $a_0=-\frac{3}{4}a^2$, $a_2=a^2/4$, $a_3=a^3\mu/3$, $\theta=\omega t+\phi$, and the ellipses correspond to higher-harmonic components. Introducing now the transformation

$$\delta x=u\exp\left[\frac{-1}{2}\int_0^t P_1(t')dt'\right], \tag{12}$$

Eq. (9) can be converted into a Hill equation

$$\ddot{u}+P(t)u=0, \tag{13}$$

where

$$P(t)=P_2-\frac{P_1^2}{4}-\frac{\dot{P}_1}{2}. \tag{14}$$

Using the form of P_1 and P_2 given in Eqs. (10) and (11), the transformation (12) can be rewritten as

$$\delta x=u\exp\left[-\Delta t+\frac{\mu}{2}\int_0^{\omega t}\left(2a_0\cos\theta+\frac{a^2}{2}\cos2\theta\right)d\theta\right], \tag{15}$$

$$\Delta=\frac{1}{2}\mu\left[\frac{a^2}{2}+a_0^2+\frac{a_2^2}{2}+\frac{a_3^2}{2}-1\right]. \tag{16}$$

Applying the Floquet theorem, one can look for a particular solution of Eq. (13) in the form

$$u=\exp(\epsilon_1 t)\phi(t), \tag{17}$$

where $\phi(t)$ is a periodic function of time and ϵ_1 is either real or imaginary. Thus Eq. (15) becomes

$$\delta x(t)=\exp(\epsilon_1-\Delta)t\overline{\phi}(t), \tag{18}$$

where

$$\overline{\phi}(t)=\phi(t)\exp\left[\frac{\mu}{2}\int_0^{\omega t}\left(2a_0a\cos\theta+\frac{a^2}{2}\cos2\theta\right)d\theta\right]. \tag{19}$$

The stability of solution (3) depends exclusively on the exponent coefficient $(\epsilon_1-\Delta)$ in Eq. (18). Let us now discuss the various possibilities to have a stable solution.

Case (i). Considering the case $\epsilon_1=\pm i\overline{\epsilon_1}$ so that $\overline{\epsilon_1}$ is real and positive, then

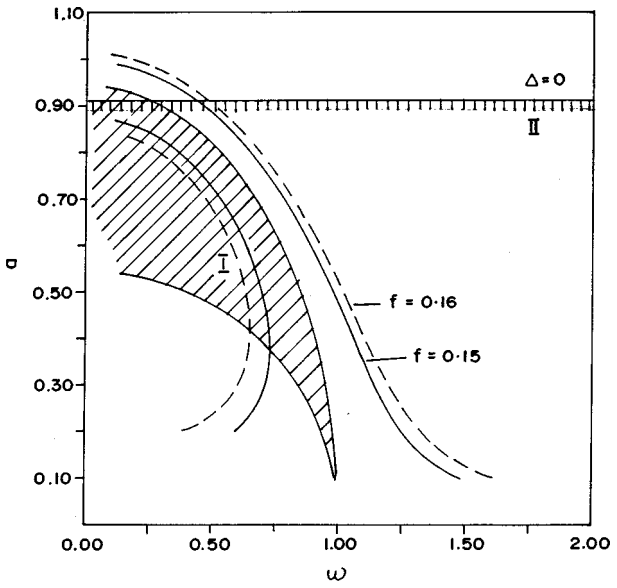

FIG. 12. Resonance curves and unstable regions of solution (3): I, branches unstable in the sense of first-order instability; II, branches unstable in the sense of Neimark instability.

$$\delta x(t)=\exp(\pm i\overline{\epsilon_1}-\Delta)t\overline{\phi}(t). \tag{20}$$

It can be concluded that when ϵ_1 is imaginary, the solution (3) is stable if $\Delta>0$ or $a>0.91$ and unstable if $\Delta<0$. This form of instability (termed Neimark instability) leads to a buildup of new harmonic components whose frequencies are incommensurate with the frequency of the periodic solution (3).

Case (ii). Considering the case $\epsilon_1=\pm\overline{\epsilon_1}$ so that $\overline{\epsilon_1}$ is real, then

$$\delta x(t)=\exp(\pm\overline{\epsilon_1}-\Delta)t\overline{\phi}(t). \tag{21}$$

When $\overline{\epsilon_1}$ is real, the solution (3) is stable if $\Delta>0$ and $\Delta^2>\overline{\epsilon}_1^2$ and this form of instability is approximately equal to the classic first-order instability as given by Eq. (7).

Therefore, the form of instability defined by Eq. (20) and so the condition $\Delta>0$ leads to the build up of new harmonic components with frequencies $\omega+\overline{\epsilon_1}$ and $\omega-\overline{\epsilon_1}$. However, these frequencies are in general incommensurate with the frequency ω of the periodic solution (3), whereas for $\Delta<0$ the solution is unstable and so $\Delta=0$ is the boundary of the instability. Thus this instability can be interpreted as a Neimark instability, giving rise to a Neimark bifurcation.

Let us now look at the resonance curves, shown in Fig. 12, and the two unstable regions defined by condition (7) (first-order instability) and the condition $\Delta<0$ for Neimark instability. From Fig. 12 the Neimark instability is expected to occur at the frequency value where the resonance curve crosses the critical boundary value $a\sim0.91$. To determine the Neimark stability limit in the f-ω parameter plane, we calculate the forcing parameter f by using the resonance equation (4). Figure 13 depicts the Neimark instability limit defined by the condition $\Delta<0$ and the first-order stability limit described by the condition (7). The numerical study results presented already in Fig. 1 are shown for comparison.

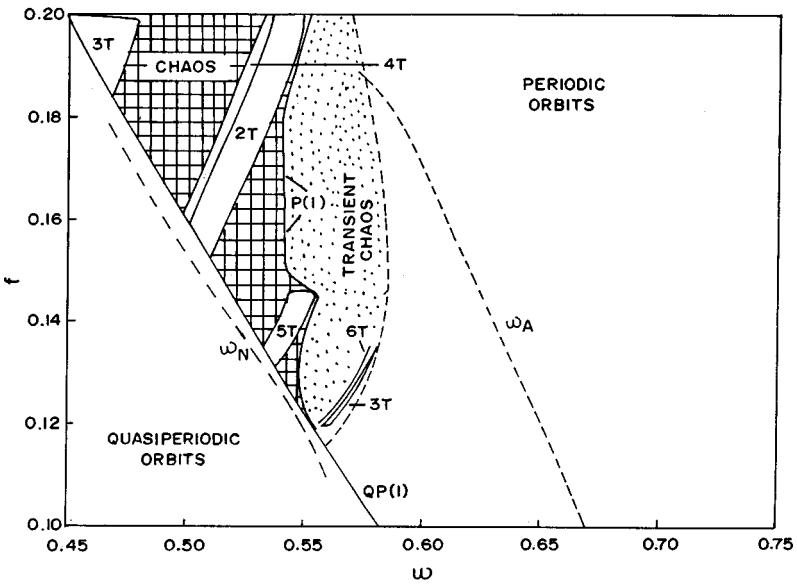

FIG. 13. Regions of different steady states: numerical (solid line) and theoretical (dashed line) stability limits.

The theoretically predicted Neimark instability values are reasonably close to the numerical results.

IV. COMPARISON OF THE DYNAMICS WITH THE DOUBLE-WELL DUFFING OSCILLATOR

Finally, it is of importance to compare the dynamics of the double-well Duffing oscillator as given by Szemplinska-Stupnika and Rudowski [15],

$$\ddot{x}+\mu\dot{x}-|\alpha|x+\beta x^3=f\cos\omega t, \tag{22}$$

with that of double-well DVP oscillator (2) for the same parametric values $|\alpha|=\beta=0.5$ and $\mu=0.1$. The results are compared in Table I. In the lower-frequency boundary region (see Fig. 1 of Ref. [15]), the Duffing oscillator exhibits symmetry-breaking bifurcations, while in the DVP oscillator, a Neimark bifurcation boundary (Fig. 1 of the present paper) has been found. In the higher-frequency boundary region, particularly in the principal resonance region, the Duffing system exhibits period-doubling bifurcations of small periodic orbits and cross-well chaos. However, in the DVP system, this region is always found to have highly regular orbits.

TABLE I. Comparison of the orbits of Duffing and DVP oscillators.

Parameters	f	Duffing oscillator	DVP oscillator
$\omega\in(0.4,0.6)$	small	small orbit	QP orbit
	large	large orbit and chaos	large orbit and chaos
$\omega\in(0.6,1.0)$	small	small orbit	QP orbit
	large	small orbit and chaos	large orbit

Further, the Duffing oscillator exhibits the period-doubling route to chaos of a large period-T orbit in the lower-frequency region, that is, $\omega<0.4$, while in the present case, the system always exhibits almost-periodic oscillations in the region. In the present case, for all transition boundaries such as QP(1), P(1), and QP(2), there are some regions where the coexistence of multiple attractors is found to occur. But in the Duffing oscillator case, the coexistence of multiple attractors is observed in the transition region from a large period-T orbit to cross-well chaos. Blue-sky catastrophes, type-II and -III intermittencies, and various phase-locked states are found to occur in the present case. However, in the Duffing oscillator case such phenomena have not been found (at least to our knowledge). Naturally, the dynamics exhibited by the DVP equation (2) is also quite distinct compared to the forced van der Pol oscillator [27].

V. CONCLUSION

Numerical studies show that the double-well Duffing–van der Pol oscillator (2) with the parameter choice $|\alpha|=\beta$ exhibits a rich variety of attractors of periodic, quasiperiodic, and chaotic types. Four varieties of transitions from quasiperiodic to periodic motions occur: (i) QP—periodic orbits (ii) QP—chaos—periodic, (iii) QP—chaos—periodic windows—chaos—periodic, and (iv) QP—phase-locked states—chaos—periodic orbits. In addition to these, local stable and supercritical, unstable and subcritical Neimark bifurcations and mode-locking, intermittent catastrophe, and blue-sky catastrophe bifurcations are also shown to exist. Transient chaos, period-doubling phenomena, boundary crises, and intermittencies of all three classic types are shown to occur and these were demonstrated with suitable examples in the f-ω parameter space. In the literature, so far all three intermittencies have been found to occur mostly in the higher-dimensional or coupled systems [21–23]. However, in the present case, even in a single model of a low-dimensional system, we are able to demonstrate all three kinds of Pomeau-Manneville intermittencies. The various

forms of instability of the approximate periodic solution allows one to predict the Neimark bifurcation in the f-ω parameter domain. Although some discrepancy between true and theoretical predictions occurs, the approximate analysis allows one to distinguish between the regular and chaotic regions.

ACKNOWLEDGMENTS

This work forms part of a Department of Science and Technology, Government of India research project. A.V. wishes to acknowledge the Council of Scientific and Industrial Research, Government of India, for providing financial support.

[1] M. Lakshmanan and K. Murali, *Chaos in Nonlinear Oscillators: Controlling and Synchronization* (World Scientific, Singapore, 1996).
[2] H. A. Haus, *Waves and Fields in Optoelectronics* (Prentice-Hall, Englewood Cliffs, NJ, 1984).
[3] B. J. A. Zielinska, D. Mukamel, V. Steinberg, and S. Fishman, Phys. Rev. A **32**, 702 (1985).
[4] P. J. Probert and J. E. Carrol, Proc. IEEE **134**, 295 (1987); **136**, 22 (1989).
[5] S. Rajasekar and M. Lakshmanan, Physica D **32**, 146 (1988).
[6] J. Guckenheimer and P. Holmes, *Nonlinear Oscillations and Bifurcations of Vector Fields* (Springer-Verlag, New York, 1983).
[7] E. Atlee Jackson, *Perspectives of Nonlinear Dynamics* (Cambridge University Press, New York, 1991).
[8] Y. Udea and N. Akamatasu, IEEE Trans. Circuits Syst. **28**, 217 (1981).
[9] W. H. Steeb and A. Kunick, Int. J. Nonlinear Mech. **22**, 349 (1987).
[10] A. S. Demitriev, U. A. Komelv, and D. Y. Turaev, Int. J. Bifurcation Chaos **2**, 93 (1992).
[11] T. C. Bountis, L. B. Drossos, M. Lakshmanan, and S. Parthasarthy, J. Phys. A **24**, 6924 (1993).
[12] W. Szemplinska-Stupnika and J. Rudowski, Phys. Lett. A **192**, 201 (1994).
[13] S. Rajasekar, S. Parthasarthy, and M. Lakshmanan, Chaos Solitons Fractals **2**, 271 (1992).
[14] Y. Kao and C. S. Wang, Phys. Rev. E **48**, 2514 (1993).
[15] W. Szemplinska-Stupnika and J. Rudowski, Chaos **3**, 376 (1993).
[16] A. Venkatesan and M. Lakshmanan (unpublished).
[17] J. M. T. Thompson and H. B. Stewart, *Nonlinear Dynamics and Chaos* (Wiley, New York, 1986).
[18] J. M. T. Thompson, Proc. R. Soc. London, Ser. A **421**, 195 (1989).
[19] Y. Pomeau and P. Manneville, Commun. Math. Phys. **74**, 189 (1980).
[20] R. H. Abraham and H. B. Stewart, Physica D **21**, 394 (1986).
[21] C. Grebogi, E. Ott, and J. A. Yorke, Physica D **7**, 181 (1983).
[22] P. Manneville and Y. Pomeau, Phys. Lett. **75A**, 1 (1979); Physica D **1**, 219 (1980).
[23] J. Y. Huang and J. J. Kim, Phys. Rev. A **36**, 1475 (1987).
[24] J. San-Martin and J. C. Antoranz, Phys. Lett. A **219**, 69 (1996).
[25] S. Chatterjee and A. K. Mallik, Phys. Rev. E **53**, 4362 (1996).
[26] A. H. Nayfeh and D. T. Mook, *Nonlinear Oscillations* (Wiley, New York, 1979).
[27] U. Parlitz and W. Lauterborn, Phys. Rev. A **36**, 1428 (1987).